Journal of Materials Chemistry C

ROYAL SOCIETY OF CHEMISTRY

PAPER

View Article Online
View Journal | View Issue

Cite this: J. Mater. Chem. C, 2022, 10, 4668

Indeno-anthraquinone hosts with thermally activated delayed fluorescence for deep-red OLEDs†

Chen Yin,[a] Ruihuan Liu,[a] Dongdong Zhang*[a] and Lian Duan *[ab]

Received 15th October 2021,
Accepted 30th January 2022

DOI: 10.1039/d1tc04962c

rsc.li/materials-c

High-efficiency materials exhibiting thermally activated delayed fluorescence (TADF) are highly promising for organic light-emitting diodes (OLEDs). A rational acceptor core based on indeno-anthraquinone (IAQ) was proposed in this work. It showed molecular ridigity and expanded conjugation for construction of orange–red TADF. Two TADF molecules involving IAQ were designed and synthesized. They simultaneously possessed high photoluminescence quantum efficiency (PLQY) and efficient reverse intersystem crossing (RISC) for red cationic iridium phosphor to construct TADF-sensitized phosphorescent (TSP) OLEDs. As a result, a stable OLED device exhibiting deep-red emission was fabricated with a maximum external quantum efficiency (EQE_{max}) of 15.1% and Commission Internationale de L'Eclairage coordinate of (0.69, 0.31).

Introduction

In recent decades, organic light-emitting diodes (OLEDs) have become next-generation technology for display and lighting. OLEDs have been applied commercially thanks to the development of emitters.[1–3] Among emitters, thermally activated delayed fluorophores are promising because of their noble metal-free character and high quantum efficiency thanks to reverse intersystem crossing (RISC) from non-radiative triplets (T_1) to radiative singlets (S_1).[3] However, the long delay originating from the S_1–T_1 cycle inhibits the intrinsic stability induced by exciton annihilation. This feature limits the further development of thermally activated delayed fluorophores, especially for those with red or deep-red emission governed by the energy gap.[4,5]

In comparison, phosphors, especially those involving iridium(III), are ideal for highly efficient and stable red OLEDs. This is ascribed to the high quantum efficiency endowed by spin-orbital coupling (SOC) of metals with a typical phosphorescent lifetime of several microseconds.[6] In general, the development of neutral iridium complexes is more mature than that of ionic complexes due to their ease of evaporation and high efficiency.[7] With increasing and persistent research efforts, sublimable ionic iridium complexes (especially cationic types) have attracted increasing attention with regard to their superior photophysical properties, facile design and electrochemical stability, there by making them promising candidates for high-performance OLEDs.[8]

However, severe aggregation-caused quenching (ACQ), inferior device efficiency and limited device stability restrict the development of sublimable cationic Ir(III) complexes as phosphorescent emitters.[9,10] In recent years, our research team has proposed an advanced strategy, thermally activated delayed fluorescence (TADF)-sensitized phosphorescence (TSP), in which bipolar materials with TADF are employed as sensitizing hosts for Ir(III)-involved phosphors.[11–14] Compared with conventional hosts showing a wide energy gap, TADF hosts exhibit suitable excited-state energy that allows a low injection barrier as well as Förster energy transfer (FET) between the host and emitter even with lower phosphor doping. Consequently, the lower on-set voltage and improved device efficiency were obtained simultaneously in TSP devices compared with phosphorescent OLEDs employing a conventional host. Simulations of exciton dynamics were undertaken and demonstrated the feasibility of TSP to improve the efficiency and stability of the device, which was ascribed to the reduced lifetime and density of triplets as well as nonradiative energy loss *via* energy transfer.[15]

In general, to guarantee ideal sensitization, TADF hosts endowing high photoluminescence quantum efficiency (PLQY), fast RISC rate (k_{RISC}) and in particular suitable emission for efficient FET are highly desired.[16] For a sublimable cationic Ir(III) complex with red emission, TADF hosts exhibiting orange-to-red shifts are highly desired in terms of spectral matches that allow effective energy transfer at low phosphor doping with alleviated ACQ character.

[a] Key Lab of Organic Optoelectronics & Molecular Engineering of Ministry of Education, Department of Chemistry, Tsinghua University, Beijing 100084, P. R. China. E-mail: ddzhang@mail.tsinghua.edu.cn, duanl@mail.tsinghua.edu.cn
[b] Center for Flexible Electronics Technology, Tsinghua University, Beijing 10084, P. R. China

† Electronic supplementary information (ESI) available. See DOI: 10.1039/d1tc04962c

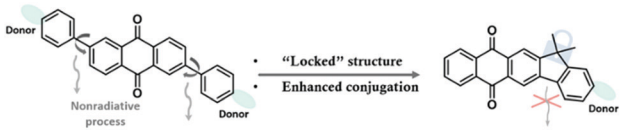

Scheme 1 Molecular structure of indeno-anthraquinone (IAQ) inspired from 2,6-diphenylanthracene-9,10-dione (AQ).

Inspired by the work of Zhang and colleagues, we designed a new acceptor based on indeno-anthraquinone (IAQ) (Scheme 1).[17] Compared with 2,6-diphenylanthracene-9,10-dione (AQ) reported by Zhang and colleagues, fewer phenyl bridges allow single substitution of a donor group so that the molecular mass can be restricted for better evaporation. Moreover, introduction of a "lock" structure not only reduces the non-radiative process induced by the relatively free rotation in the AQ skeleton, it also increases the overall conjugation for red-shift emission. As illustrated in Fig. 1, two molecules (IAQ-PhCz and IAQ-CzCz) with orange emission were designed based on an IAQ acceptor, accompanied with high PLQYs and fast RISC. In this work, $[Ir(dpq)_2(bpy)][B(5FPh)_4]$, a newly designed sublimable cationic Ir(III) complex created by our research team, was employed as the red emitter in terms of its high quantum efficiency and suitable absorption spectra.[18] As a result, highly efficient OLED endowing an EQE_{max} of 15.1%, Commission Internationale de L'Eclairage (CIE) coordinate of (0.69, 0.31) and reduced efficiency roll-off was constructed. This work provides a new type of acceptor based on IAQ for orange–red TADF materials, and promises a solution for high-performance phosphorescent OLEDs based on a sublimable ionic Ir(III) complex with red emission.

Results and discussion

Theoretical calculation

Molecular optimizations were undertaken and orbital distribution of ground states identified by Gaussian 09 utilizing B3LYP/6-31G(d) for both molecules. In addition, excitation energies were calculated by means of time dependent-density functional theory (TD-DFT) employing B3LYP/6-31G(d). As illustrated in Fig. 1, the highest occupied molecular orbitals (HOMOs) were mostly localized on overall donor structures and partially on the indeno-phenyl group, whereas the lowest unoccupied molecular orbitals (LUMOs) were entirely on IAQ groups for IAQ-PhCz and IAQ-CzCz, which indicated a small orbital overlap. The calculated excitation energy for the lowest singlet (S_1)/triplet (T_1) of IAQ-PhCz and IAQ-CzCz was 2.19/2.08 and 2.09/2.06 eV with a corresponding energy gap (ΔE_{ST}) of 0.11 and 0.03 eV, respectively, which suggested a possible TADF property.

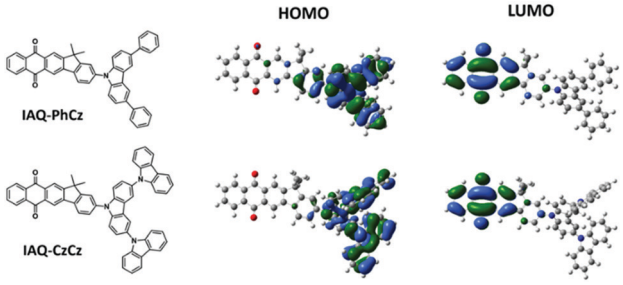

Fig. 1 Molecular structure and simulated HOMO/LUMO orbital distributions of IAQ-PhCz and IAQ-CzCz.

Synthesis and characterization

Both molecules were synthesized by one-step C–N coupling between 2-bromo-13,13-dimethyl-6*H*-indeno[1,2-*b*]anthracene-6,11(13*H*)-dione (IAQ–Br) and carbazole derivatives. More details can be found in ESI.†

Thermal stability and electrochemical property

Thermogravimetric analysis (TGA) and differential scanning calorimetry (DSC) were undertaken to evaluate molecular thermal stability. As illustrated in Fig. S1, (ESI†) IAQ-PhCz and IAQ-CzCz exhibited significant stability, of which the decomposition temperature (Td, which corresponded to 5 wt% loss) was 429 and 449 °C, respectively. DSC traces (Fig. S2, ESI†) revealed the phase transitions for both materials, with the corresponding glass transition temperature being 181 °C for IAQ-PhCz and 235 °C for IAQ-CzCz. Hence, both molecules appeared to have good thermal stability.

The specific energy of HOMO/LUMO was obtained by cyclic voltammetry, and was −5.9/−3.4 eV for IAQ-PhCz and −6.0/−3.4 eV for IAQ-CzCz (Fig. S3, ESI†). With regard to reductive curves, similar patterns were recorded for both molecules, which could be ascribed to the IAQ group. In contrast, the two materials endowed different oxidative curves induced by specific donors.

Photophysical properties

For both materials, the absorption, photoluminescence (PL) and phosphorescence spectra were measured in toluene solution in air at a concentration of 10^{-5} M (Fig. 2a and b). There were three dominant absorption peaks for IAQ-PhCz and IAQ-CzCz. The highest one peaked at ~290 nm and was ascribed to the π–π* transition of the phenyl group. The middle peak was attributed to the carbazole n–π* transition. The lowest peak was attributed to the intramolecular charge transfer (CT) between the acceptor and donor.[19] Both molecules exhibited featureless and broad PL spectra with peak emission of 552 nm for IAQ-PhCz and 560 nm for IAQ-CzCz, which suggested typical CT-type emission. Tangents were made to determine the S_1 energy for both molecules: it was 2.54 eV. For the phosphorescence spectra measured at 77 K, IAQ-PhCz showed a curve with fine structures but weak features for IAQ-CzCz; the corresponding T_1 and ΔE_{ST} energy was 2.40/2.46 eV and 0.14/0.08 eV, respectively. PLQY of 0.70 for IAQ-PhCz and 0.83 for IAQ-CzCz was found in degassed toluene solution at a concentration of 10^{-5} M, which validated the design strategy based on the "locked" acceptor.

Given the practical applications of TADF materials as aggregates in OLEDs, their photophysical properties were studied further in doped films utilizing mCP as the matrix host. The PL spectra of 10 wt%-doped film are illustrated in Fig. 2c. IAQ-PhCz

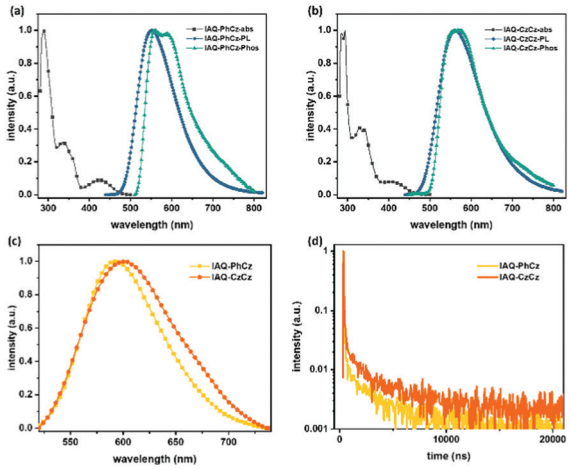

Fig. 2 Photophysical properties of IAQ-PhCz and IAQ-CzCz. The absorption (Abs), photo-luminance (PL) and low-temperature phosphorescence (Phos) spectra of (a) IAQ-PhCz and (b) IAQ-CzCz in toluene solution at ambient conditions. (c) PL spectra and (d) PL transient decay curves of mCP-doped films with 10 wt% of IAQ-PhCz/IAQ-CzCz.

peaked at 592 nm and IAQ-CzCz peaked at 602 nm, which showed a red-shift of ~40 nm compared with that observed in toluene solution. The PL spectra of TADF-films with different doping concentrations are summarized in Fig. S4, and revealed a red-shift with increasing doping for both materials. This feature could be ascribed to the enhanced intermolecular π–π interaction of IAQ components with increasing doping.[20]

Moreover, PL transient decays were studied for both molecules in mCP films with doping of 10 wt%. As illustrated in Fig. 2d, the decay curves were fitted well by two exponentials, of which the prompt lifetime and delayed lifetime was 32/35 ns and 6.45/6.44 μs for IAQ-PhCz and IAQ-CzCz, respectively, thereby suggesting a TADF property. Furthermore, the PLQY of doped films was measured without/with N_2 protection: 0.28/0.49 and 0.21/0.59 for IAQ-PhCz and IAQ-CzCz, respectively, were documented. ACQ was demonstrated in both molecules, accompanied with a spectral red-shift compared with that observed in toluene solution. The dynamic rate constant was calculated (Table 1), and a high RISC rate (k_{RISC}) was indicated for IAQ-PhCz (1.6×10^5 s^{-1}) IAQ-CzCz (3.5×10^5 s^{-1}).[21] PL transient decay curves with different doping levels are shown in Fig. S4 (ESI†). The delayed lifetime decreased with increasing doping without eliciting significant changes in the prompt lifetime, which further verified the TADF properties for both molecules. The similarly high PLQYs, fast radiative rates (k_rs) and k_{RISC}s for IAQ-PhCz and IAQ-CzCz suggested that they could be promising TADF hosts.

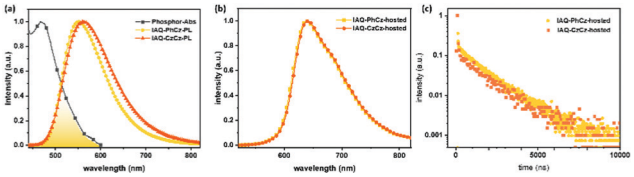

Fig. 3 Photophysical properties of 8 wt% [Ir(dpq)$_2$bpy][B(5FPh)$_4$]-doped films in IAQ-PhCz and IAQ-CzCz. (a) FET evaluation between phosphor and IAQ derivatives, (b) PL spectra of doped films, and (c) PL transient decay curves measured at 640 nm.

As TADF hosts for [Ir(dpq)$_2$(bpy)][B(5FPh)$_4$]

To endow efficiency in TSP systems, efficient FET between the TADF host and phosphor is required. A sublimable cationic Ir(III) complex with deep-red emission, [Ir(dpq)$_2$(bpy)][B(5FPh)$_4$], was selected as the final emitter with regard to the spectral match. FET evaluation was carried out as illustrated in Fig. 3a. Absorption spectra and PL spectra were recorded in toluene solution for FET calculation. Importantly, spectral overlap was noted between the absorption curves of the Ir-complex and the PL spectra of IAQ-PhCz and IAQ-CzCz, with large FET radii of 3.33 and 3.34 nm, respectively.[22] Hence, [Ir(dpq)$_2$(bpy)][B(5FPh)$_4$] was selected as the emitter. Moreover, the photophysical properties of spin-coated TADF-hosted [Ir(dpq)$_2$(bpy)][B(5FPh)$_4$] films were studied at a doping concentration of 8 wt%. PL spectra are shown in Fig. 3b, in which typical red emission from [Ir(dpq)$_2$(bpy)][B(5FPh)$_4$] with a peak ~640 nm was detected in both systems, which suggested complete energy transfer. Furthermore, there was a subtle spectral red-shift in IAQ-CzCz-film compared with that in IAQ-PhCz-film, which could be attributed to the different polarity of the host.

PL transient decay curves were recorded at a monitoring wavelength of 640 nm (Fig. 3c). Prompt and delayed parts were recognized for both systems, in which the former was ascribed to the radiative emission of the TADF host whereas the latter was from the phosphorescence of phosphor. The similar delayed curves indicated that the FET processes and RISC in both systems were more efficient than the radiative decay of phosphor. Previously, we demonstrated that phosphor could induce an external heavy atom (EHA) effect that would accelerate the RISC in a TADF host.[23] As a result, significant exciton dynamics were not observed under the photoluminescence condition. However, the original ratio of host triplets would increase markedly under electroluminescence governed by the spin rule. This phenomenon indicates the importance of the RISC process, which determines the overall dynamics. Given that IAQ-CzCz exhibited a faster k_{RISC} as well as FET than that of IAQ-PhCz, IAQ-CzCz could be a promising host.[24] Moreover, an

Table 1 Photophysical properties of mCP-doped films with 10 wt% of IAQ-PhCz and IAQ-CzCz, respectively

	λ_{max} (nm)	τ_P (ns)	τ_D (μs)	Φ_P (%)	Φ_D (%)	k_r (10^6 s^{-1})	k_{nr} (10^6 s^{-1})	k_{ISC} (10^7 s^{-1})	k_{RISC} (10^5 s^{-1})
IAQ-PhCz	592	32	6.45	0.28	0.21	8.7	1.1	2.3	1.6
IAQ-CzCz	602	35	6.44	0.21	0.38	6.1	0.8	2.3	3.5

improved PLQY was realized after doping of the Ir complex, with a value of 0.62 and 0.74 for IAQ-PhCz- and IAQ-CzCz-based films, respectively. These data suggested inhibition of nonradiative energy loss of TADF materials *via* FET. The results shown above suggested the feasibility of a TSP strategy employing IAQ-PhCz and IAQ-CzCz as hosts for $[Ir(dpq)_2(bpy)][B(5FPh)_4]$.

Device performance

OLED devices featuring a structure of ITO/HAT (5 nm)/NPB (30 nm)/TCTA (10 nm)/emitting layer (EML) (30 nm)/BPBiPA (30 nm)/LiF (0.6 nm)/Al (150 nm) were constructed. In these devices: ITO was Indium tin oxide; HAT was 1,4,5,8,9,11-hexaazatriphenylenehexacarbonitrile; NPB was 4,4′-*N*,*N*′-bis[*N*-(1-naphthyl)-*N*-phenylamino]biphenyl; TCTA was tris(4-(9*H*-carbazol-9-yl)phenyl)amine; BPBiPA was 9,10-bis(4-(2-phenyl-1*H*-benzo[*d*]imidazol-1-yl)phenyl)anthracene. The molecular structures and energy-level diagrams of devices are shown in Fig. 4a. Optimization of emitter doping was undertaken, and device performances are illustrated in Fig. S8. By virtue of the difficulty of evaporation of $[Ir(dpq)_2(bpy)][B(5FPh)_4]$, its ionic character and high molecular mass, the doping concentration is optimized at ~1 wt% in practice. As a result, the IAQ-PhCz-hosted device 1 employed a phosphor doping of 1.2 wt% whereas the IAQ-CzCz-based device 2 employed a phosphor doping of 1.4 wt%.

The specific performances of both devices are indicated in Fig. 4 and summarized in Table 2. The luminance–voltage–current density (*L*–*V*–*J*) curves are shown in Fig. 4b. Importantly, both devices revealed high maximum luminance (L_{max}) of 26 078 and 19 633 cd m^{-2} for device 1 and device 2, respectively. Importantly, there was remarkable difference in electrical performance between two devices. To further understand this phenomenon, hole-only-devices (HODs) and electron-only-devices (EODs) were fabricated for IAQ-PhCz and IAQ-CzCz, respectively. The current density–voltage (*J*–*V*) curves are illustrated in Fig. S7 (ESI†) and suggest that IAQ-PhCz exhibited relatively balanced transportation of holes and electrons. In comparison, IAQ-CzCz suffered from inferior transportation of electrons compared with hole transportation, which induced higher driving voltages than those of IAQ-PhCz.

In terms of device efficiency, a high maximum external quantum efficiency (EQE_{max}) of 14.2% was recorded for device 1 and 15.1% in device 2, both of which were higher than a device employing DIC-TRZ as a sensitizing host (10.3%) in previous work.[18] However, device 1 suffered from a remarkable roll-off, for which the EQE dropped to 58% of the maximum at 10 000 cd m^{-2}. By comparison, device 2 endowed a reduced efficiency roll-off, with EQE remaining ~79% of the EQE_{max} at identical luminance, which showed superior stability compared with reported OLEDs with cationic Iridium phosphor.[18] This feature could be due to the fast dynamics ascribed to the high k_{RISC} of IAQ-CzCz. Besides, the maximum value of current efficiency (CE) and power efficiency (PE) was 10.2/9.1 cd A^{-1} and 10.1/7.6 lm W^{-1} for device 1 and device 2, respectively.

Electroluminescence spectra are illustrated in Fig. 4d. The peak emission was located at 637 nm in device 1 and 640 nm in device 2, similar to the PL emission in doped films (Fig. 3b). Energy transfer from the TADF host to $[Ir(dpq)_2(bpy)][B(5FPh)_4]$ was complete, and negligible host emission was recognized in both devices. As depicted in Fig. 4e, the corresponding CIE coordinates were (0.67, 0.32) and (0.69, 0.31) for device 1 and device 2, respectively. In particular, device 2 achieved red emission over the National Television System Committee (NTSC) recommended standard, indicating ideal colour purity.

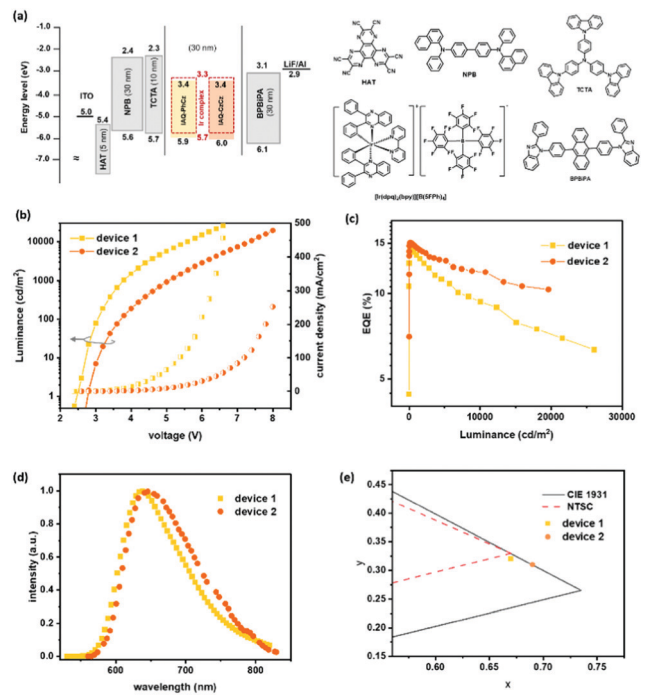

Fig. 4 Structure and performance of devices. (a) Energy diagrams and molecular structures, (b) Luminance–voltage–current density (*L*–*V*–*J*) curves, (c) EQE *versus* luminance curves and (d) electroluminescence spectra monitored at 1000 cd m^{-2} of device 1 and device 2. (e) CIE coordination including NTSC and CIE 1931 standard.

Experimental sections

General information

Commercial reagents were used without purification. Molecular characterizations were undertaken by matrix-assisted laser desorption ion-trap (MALDI) mass spectroscopy (Schimadzu, Japan) without a matrix as well as ^1H and ^{13}C nuclear magnetic resonance (NMR) spectroscopy with a 600 MHz spectrometer (Bruker, USA) employing tetramethylsilane (TMS) as the internal standard.

TGA and DSC were carried out with TGA Q5000 (TA Instruments, USA) and DSC Q2000 (TA Instruments) systems, respectively. Cyclic-voltammetry curves were recorded by a three-electrode electrochemical station (CHI600E; CH Instruments, USA) with a scan rate of 0.1 V s^{-1}, for which anhydrous *N*,*N*-dimethylformamide (DMF) and dichloromethane (DCM) were applied for reductive and oxidative potentials,

Table 2 Summary of device performances

		EQE (%)			Current efficiency (cd A^{-1})					
Device	V_{on} (V)	Max	At 1000 cd m^{-2}	At 10 000 cd m^{-2}	Max	At 1000 cd m^{-2}	At 10 000 cd m^{-2}	L_{max} (cd m^{-2})	EL peak (nm)	CIE
1	2.46	14.2	13.7	9.4	10.4	10.2	7.9	26 078	637	0.67, 0.32
2	2.77	15.1	14.6	11.9	9.6	9.6	8.7	19 633	640	0.69, 0.31

respectively. In addition, ferrocene/ferrocenium was employed as the standard.

Ultraviolet-visible (UV-vis) absorption curves were obtained using a spectrophotometer (8453; Agilent Technologies, USA). Photoluminescence and low-temperature phosphorescence spectra were determined using an LP920-KS fluorescence spectrophotometer (Edinburgh Instruments, UK). PLQYs and device performances were determined using a C9920-02 system (Hamamatsu Photonics, Japan). PL transient decay curves were recorded by a FLS1000 transient spectrometer (Edinburgh Instruments).

OLED fabrication

Before device fabrication, ITO glass was precleaned and dried. TADF molecules and the Ir(III) complex were purified by vacuum sublimation. OLED devices were fabricated under a pressure of $\sim 10^{-6}$ Torr. Organic layers were constructed with an evaporation rate of 0.5–1 Å s^{-1}, whereas LiF was 0.02 Å s^{-1} and Al was 2 Å s^{-1}. After cooling for 30 min in a vacuum, the devices were characterized without encapsulation.

Conclusions

We designed a new acceptor IAQ based on anthraquinone, which endowed molecular rigidity and high conjugation for inhibition of non-radiative energy loss and red-shift emission. Then, two TADF molecules with orange emission as well as high PLQY and k_{RISC}, IAQ-PhCz and IAQ-CzCz, were designed and synthesized. Employing these materials as sensitizing hosts for a sublimable cationic Ir(III) complex, $[Ir(dpq)_2(bpy)][B(5FPh)_4]$, TSP devices were fabricated, among which a high EQE_{max} of 15.1% and reduced efficiency roll-off was realized. We demonstrated the feasibility of the acceptor design and provided a robust strategy for high-performance phosphorescent OLEDs employing sublimable cationic phosphors.

Author contributions

Chen Yin and Ruihuan Liu contributed equally to this work.

Conflicts of interest

There are no conflicts to declare.

Acknowledgements

This study was supported financially by the Guangdong Major Project of Basic and Applied Basic Research (2019B030302009), National Key Basic Research and Development Program of China (2020YFA0715000 and 2017YFA0204501), National Natural Science Foundation of China (22135004, 51903137 and 61890942), Young Elite Scientists Sponsorship Program by CAST (2019-2021QNRC) and Tsinghua-Foshan Innovation Special Fund (2020THFS0116).

Notes and references

1 C. W. Tang and S. A. VanSlyke, *Appl. Phys. Lett.*, 1987, **51**, 913–915.
2 Y. Huang, E.-L. Hsiang, M.-Y. Deng and S.-T. Wu, *Light: Sci. Appl.*, 2020, **9**, 1–16.
3 D. Zhang, T. Huang and L. Duan, *Adv. Mater.*, 2020, **32**, 1902391.
4 C. Baleizão and M. N. Berberan-Santos, *J. Chem. Phys.*, 2007, **126**, 204510.
5 J. V. Caspar, E. M. Kober, B. P. Sullivan and T. J. Meyer, *J. Am. Chem. Soc.*, 1982, **104**, 630–632.
6 C.-L. Ho, H. Li and W.-Y. Wong, *J. Organomet. Chem.*, 2014, **751**, 261–285.
7 B. Powell, *Coord. Chem. Rev.*, 2015, **295**, 46–79.
8 D. Ma, T. Tsuboi, Y. Qiu and L. Duan, *Adv. Mater.*, 2017, **29**, 1603252.
9 C. Murawski, K. Leo and M. C. Gather, *Adv. Mater.*, 2013, **25**, 6801–6827.
10 J. Ribierre, A. Ruseckas, K. Knights, S. Staton, N. Cumpstey, P. Burn and I. Samuel, *Phys. Rev. Lett.*, 2008, **100**, 017402.
11 D. Zhang, L. Duan, D. Zhang, J. Qiao, G. Dong, L. Wang and Y. Qiu, *Org. Electron.*, 2013, **14**, 260–266.
12 D. Zhang, L. Duan, Y. Li, H. Li, Z. Bin, D. Zhang, J. Qiao, G. Dong, L. Wang and Y. Qiu, *Adv. Funct. Mater.*, 2014, **24**, 3551–3561.
13 D. Zhang, L. Duan, D. Zhang and Y. Qiu, *J. Mater. Chem. C*, 2014, **2**, 8983–8989.
14 Y. Li, D. Zhang and L. Duan, *Org. Electron.*, 2018, **57**, 53–59.
15 C. Li, L. Duan, D. Zhang and Y. Qiu, *ACS Appl. Mater. Interfaces*, 2015, **7**, 15154–15159.
16 M. Cai, D. Zhang and L. Duan, *Chem. Rec.*, 2019, **19**, 1611–1623.
17 Q. Zhang, H. Kuwabara, W. J. Potscavage, Jr., S. Huang, Y. Hatae, T. Shibata and C. Adachi, *J. Am. Chem. Soc.*, 2014, **136**, 18070–18081.
18 R. Liu, D. Ma and L. Duan, *J. Mater. Chem. C*, 2020, **8**, 14766–14772.

19 J.-R. Cha, C. W. Lee, J. Y. Lee and M.-S. Gong, *Dyes Pigm.*, 2016, **134**, 562–568.
20 J. Xue, Q. Liang, R. Wang, J. Hou, W. Li, Q. Peng, Z. Shuai and J. Qiao, *Adv. Mater.*, 2019, **31**, e1808242.
21 K. Masui, H. Nakanotani and C. Adachi, *Org. Electron.*, 2013, **14**, 2721–2726.
22 B. W. D'Andrade, M. A. Baldo, C. Adachi, J. Brooks, M. E. Thompson and S. R. Forrest, *Appl. Phys. Lett.*, 2001, **79**, 1045–1047.
23 D. Zhang, L. Duan, Y. Zhang, M. Cai, D. Zhang and Y. Qiu, *Light: Sci. Appl.*, 2015, **4**, e232.
24 C. Yin, D. Zhang, Y. Zhang, Y. Lu, R. Wang, G. Li and L. Duan, *CCS Chem.*, 2020, **2**, 1268–1277.